

Improving Road Semantic Segmentation Using Generative Adversarial Network

ABOLFAZL ABDOLLAHI¹, (STUDENT MEMBER, IEEE), BISWAJEET PRADHAN^{1,2,3*}, (SENIOR MEMBER, IEEE), GAURAV SHARMA⁴, KHAIRUL NIZAM ABDUL MAULUD^{3,5}, ABDULLAH ALAMRI⁶

¹Centre for Advanced Modelling and Geospatial Information Systems (CAMGIS), School of Information, Systems and Modelling, Faculty of Engineering & IT, University of Technology Sydney (UTS), NSW 2007, Australia

²Department of Energy and Mineral Resources Engineering, Sejong University, Choongmu-gwan, 209 Neungdong-ro, Gwangjingu, Seoul 05006, Korea

³Earth Observation Centre, Institute of Climate Change, Universiti Kebangsaan Malaysia, 43600 UKM, Bangi, Selangor, Malaysia

⁴Department of Electrical and Computer Engineering, University of Rochester, Rochester, NY 14627, USA

⁵Department of Civil Engineering, Faculty of Engineering and Built Environment, University Kebangsaan Malaysia, 43600 UKM Bangi, Selangor, Malaysia

⁶Department of Geology and Geophysics, College of Science, King Saud University, P.O. Box 2455, Riyadh 11451, Saudi Arabia

*Correspondence: biswajeet24@gmail.com or Biswajeet.Pradhan@uts.edu.au

This research is supported by the Centre for Advanced Modelling and Geospatial Information Systems (CAMGIS), Faculty of Engineering and IT, University of Technology Sydney (UTS). This research is also supported by Researchers Supporting Project number RSP-2020/14, King Saud University, Riyadh, Saudi Arabia. This research also was supported by Universiti Kebangsaan Malaysia, DANA IMPAK PERDANA with Grant No: DIP-2018-030.

ABSTRACT Road network extraction from remotely sensed imagery has become a powerful tool for updating geospatial databases, owing to the success of convolutional neural network (CNN) based deep learning semantic segmentation techniques combined with the high-resolution imagery that modern remote sensing provides. However, most CNN approaches cannot obtain high precision segmentation maps with rich details when processing high-resolution remote sensing imagery. In this study, we propose a generative adversarial network (GAN)-based deep learning approach for road segmentation from high-resolution aerial imagery. In the generative part of the presented GAN approach, we use a modified UNet model (MUNet) to obtain a high-resolution segmentation map of the road network. In combination with simple pre-processing comprising edge-preserving filtering, the proposed approach offers a significant improvement in road network segmentation compared with prior approaches. In experiments conducted on the Massachusetts road image dataset, the proposed approach achieves 91.54% precision and 92.92% recall, which correspond to a Mathews correlation coefficient (MCC) of 91.13%, a Mean intersection over union (MIOU) of 87.43% and a F1-score of 92.20%. Comparisons demonstrate that the proposed GAN framework outperforms prior CNN-based approaches and is particularly effective in preserving edge information.

INDEX TERMS GAN; road segmentation; remote sensing; deep learning; U-Net

I. INTRODUCTION

Compared with aerial images that are typically restricted to three red, green, and blue (RGB) spectral channels and available for limited geographic areas, satellite imagery commonly includes further spectral channels and provides almost worldwide coverage at high resolution [1]. High-resolution remote sensing imagery is therefore an attractive option for extracting road segments to aid the development of maps for geospatial information systems (GIS) users, transportation practitioners, geodetic researchers, and urban/municipal planners and officers [2-4]. Although the 0.5–1 meter per pixel resolution for high-quality satellite images is worse than the resolution for aerial images, it is adequate for extracting road sections. However, shadows, overlapping,

interlacing, and shadowing in satellite images [5] make road segment extraction challenging [6]. The manual segmentation of roads is feasible based on careful examination of images, but such segmentation is costly, time-consuming, and prone to errors due to its tedious nature [7]. Thus, automatic means are necessary for accurately extracting road segments from high-resolution remote sensing imagery [8]. Machine learning-based approaches have recently demonstrated significant successes in the fields of image segmentation [9, 10], object detection [11, 12], and image classification [13, 14]. For example, in a study conducted by [15], a road detection method using maximum likelihood technique, morphological operators and Random Sample Consensus (RANSAC) has been proposed to identify the road network from Quickbird images. Another work [16] applied a hybrid road detection technique on the basis of

Trainable Weka Segmentation (TWS) and Level Set (LS) algorithms to extract roads from UAV images. A new method based on a hierarchical graph with Gabor and morphological filtering was proposed in [17] to extract roads from aerial and Quick-Bird imagery. Da-Ming, et al. [18] applied a hybrid approach combining of Markov random fields (MRFs), support vector machine (SVM) and fuzzy c-means (FCM) to extract the road network from Google Earth imagery. A new technique for road extraction from IKONOS, Quick-Bird and GeoEye imagery was also implemented in [19]. Bakhtiari, et al. [20] implemented a semi-automatic technique based on edge detection, SVM and morphological filtering to detect different road types from UltraCam airborne, Worldview and Quick-Bird imagery. However, most of the traditional machine learning approaches cannot handle multiscale road sections, especially narrow road parts with high width variation, and failed to obtain high precision in road network segmentation. Thus, for extracting semantic information and learning hierarchical features automatically from raw data, researchers are increasingly resorting to deep learning methods [21, 22]. A key reason is that deep neural networks can effectively learn from the large-scale data sets becoming available in remote sensing, such as light detection and ranging (LiDAR) point clouds, high-spatial and spectral resolution images, and multi-spectral imagery [23, 24].

Several prior works attempted to extract road parts from high-resolution remotely sensed images, including traditional and modern deep learning approaches [17]. To provide context for our presentation, we summarize previous works using deep learning approaches for road extraction in remote sensing images. Wang, et al. [25] described a semi-automatic approach based on a deep convolutional neural network (DNN) and finite state machine (FSM) consisting of two principal stages, namely, training and tracking for road extraction from high-resolution remote sensing images. In the training stage, the network was trained for identifying input image patterns associated with the FSM using high-resolution images and associated vector road maps. In the tracking stage, the FSM uses the recognized patterns to update the state and track the road segments. Although the approach is more accurate than some traditional methods, it cannot efficiently extract road parts from complex scenes where road sections are covered by obstacles. Li, et al. [26] implemented a CNN-based method for detecting roads from GeoEye and Pleiades-1A satellites with a spatial resolution of 0.5 meters. A CNN was first used to assign labels to every pixel and to predict the likelihood of each pixel being associated with a road segment. A line-integral convolutional-based technique was then used to retain edge information, connect small gaps, and obtain a smooth map. Road centerlines were finally obtained via image processing.

Results showed that the technique provides high specificity while achieving low sensitivity. Zhong, et al. [23] proposed a CNN-based method to exploit road and building features from the Massachusetts dataset that combines high-level semantic meaning and low-level fine-grained features. Additional hyper-parameters, such as training epoch, learning rate, and input image size, were also investigated to characterize the performance of the approach in the context of high-resolution remote sensing images. By combining a novel four-stride pooling layer output and the last score layer from a pre-trained fully connected network (FCN), the model accuracy remarkably improved to 78%. Panboonyuen, et al. [27] used a technique based on a deep encoder-decoder neural network (DCED) to detect road parts in the Massachusetts road dataset. They improved their proposed approach by using an exponential linear unit activation function, instead of the traditional rectified linear unit (ReLU), by incrementally rotating images in eight steps to augment training data, and by adopting a landscape metrics approach to reduce false road pixels and increase the overall efficiency. The resulting technique outperformed prior state-of-the-art approaches for road extraction from remote sensing images. In another work, [28] performed nonlocal LinkNet with nonlocal blocks (NLBs) to capture relations between global features and extract road from DeepGlobe road dataset efficiently. Cheng, et al. [29] suggested a novel deep learning approach named cascaded end-to-end (CasNet) CNN to identify road pixels and extract road centerlines from high-resolution remotely sensed imagery. Data augmentation and regularization techniques were implemented to decrease over-fitting. While useful for road recognition, the approach fails in regions where roads are surrounded by trees which cause occlusion. A novel deep learning-based approach named densely connected convolutional networks (DenseNet) was designed by [30] along with introducing global and local attention units to effectively detect road from Google Earth imagery. The results demonstrated that the proposed framework is successful and feasible in enhancing the efficiency of road semantic segmentation.

Further high-level semantic information is needed to improve the performance of road detection and to better handle occlusions. Therefore, we adopt a generative adversarial network (GAN) framework [16] to address road segmentation from remote sensing imagery. In the context of our problem setting, a GAN combines a generative network that extracts a putative road network from an input remote sensing image with a discriminator network that attempts to distinguish between road networks produced by the generator and those from ground truth labels. The generator and discriminator networks are co-optimized in a max-min setting where generator

produces the best possible road map that is maximally confusing for the discriminator that is attempting to minimize its error. Only a few works on semantic segmentation exist for road part semantic segmentation based on the GAN model. In a recent work, Luc, et al. [31] applied a GAN for segmentation and found that by enforcing the long-range spatial contiguity of labels, the model can produce smooth and precise road networks compared with non-adversarial training. However, the segmentation boundary was quite unclear, as low-level features were used by the generative model to produce the segmentation map. To overcome this limitation and to obtain a high-resolution segmentation of the road network, we propose to use a modified U-Net as the generator network.

The main contribution of this research lies in proposing a GAN with a modified U-Net generative model to extract roads from high-resolution aerial imagery. Compared to prior GAN-based road extraction approaches such as GAN+FCN proposed by [32], GAN+SegNet presented by [21], Ensemble Wasserstein Generative Adversarial Network (E-WGAN) proposed by [33], Multi-supervised Generative Adversarial Network (MsGAN) performed by [34], and Multi-conditional Generative Adversarial Network (McGAN) implemented by [35], we introduce the modified U-Net model (MUNet) for the generative term to create a high-resolution smooth segmentation map, with high spatial consistency and clear segmentation boundaries. The proposed model does not require high computational time and a large training dataset and still improves performance and addresses the aforementioned challenges for road extraction from remote sensing imagery. Also, compared with other comparative techniques that failed to refine the imperfect structures of roads, the proposed method in the current study preserves the edges and structure of roads and generates high-quality road segmentation maps in agreement with ground truth labels. The rest of the paper is organized as follows: Section II illustrates the methodology of the proposed model for road semantic segmentation and explains the dataset preparation. Section III presents the experimental results obtained using the proposed approach. Section IV compared the proposed approach against other state-of-the-art methods. Section V summarizes the conclusions.

II. METHODOLOGY

Figure 1 shows the overall methodology for training and evaluating the proposed GAN-based approach for road network extraction organized as four major steps: (i) generation of training and testing samples; (ii) local Laplacian filtering (LLF)-based pre-processing to enhance image quality; (iii) GAN optimization using the training samples, and extraction of the road network from images in the test set using the generator

from the optimized GAN; and (iv) performance quantification for the proposed method using common metrics.

A. Pre-processing

As a pre-processing step, we use LLF to enhance the quality of images prior to using them in the proposed model for training/testing. LLF is a nonlinear image filtering framework based on Laplacian pyramids (LP) that enables edge-aware processing using simple local processing operations. The filtered LLF image is obtained by rendering its LP coefficient by coefficient based on locally adaptive processing of the input image [36]. LLF was introduced in [37], where it was verified that this filtering technique can enrich image details without introducing halos or other artifacts and can be effectively used for range compression and tone mapping. With appropriate approximation and parallel implementation, LLF can be significantly speeded up to enable interactive use [36].

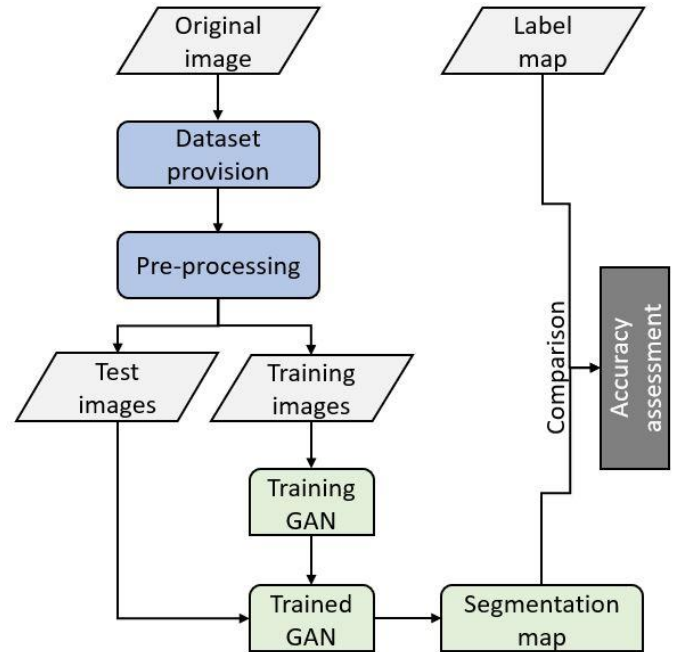


FIGURE 1. Workflow for training and evaluating the proposed approach.

B. GAN Framework for semantic segmentation

As illustrated in Fig. 2, the GAN framework [38] uses two subnetworks: a generator G and a discriminator D . The generator attempts to generate data representative of the ground truth provided for training, whereas the discriminator attempts to distinguish true ground truth data from data produced by the generator. The two subnetworks are jointly trained in an adversarial game to obtain the min-max operating point where the road maps created by G minimize the maximum discrepancy for D between the true and generated pairs. Figure 3 illustrates the detailed network architecture illustrating the structure of the generator and discriminator. For the generator,

we utilized the MUNet model that includes two corresponding arms, a contracting (downsampling) encoder and an expanding (upsampling) decoder, with skip-connections that append every upsampled feature map at the decoder with the corresponding one in the encoder that has the same spatial resolution [39].

The generator subnetwork seeks to learn a map $G : x \rightarrow y$ that produces a binary segmentation map y from the input image x based on the distribution P seen in the training data. The discriminator maps a pair $\{x, y\}$ comprised of an input image and a segmentation map to a value between 1 and 0 indicating the discriminators' estimate of whether y represents a ground truth mask or an estimate from a generator subnetwork.

For road map segmentation, the GAN objective function is then formulated as

$$L_{GAN}(G, D) = E_{x, y \sim P_{data}(x, y)} [\log D(x, y)] + E_{x \sim P_{data}(x)} [\log(1 - D(x, G(x)))] \quad (1)$$

Note that maximization of the objective function aligns with maximization of $D(x, y)$ and minimization of $D(x, G(x))$, which seeks to train the discriminator subnetwork D to make right decision. On the other hand, the generator subnetwork G should generate outputs that are indistinguishable from the true data to hamper the discriminator D from making right decision and should therefore be chosen to minimize the objective function. We defined the objective function as minimax of the objective function in (1) with maximization over choices of D and minimization over choices of G , as the final purpose is to achieve realistic probability outputs from G .

In addition to the GAN objective function, we also used a second binary cross-entropy loss function that is common in segmentation and has also recently been incorporated in a GAN framework for segmentation [39] of retinal images,

$$L_{SEG}(G) = E_{x, y \sim P_{data}(x, y)} [-y \cdot \log G(x) - (1 - y) \cdot \log(1 - G(x))] \quad (2)$$

Combining both the segmentation loss and the GAN objective function, the optimal generator network for road map segmentation is obtained as

$$G^* = \arg \min_G [\max_D L_{GAN}(G, D)] + \lambda L_{SEG}(G) \quad (3)$$

where the impact of the two objective functions can be balanced by the weighting parameter λ . In practice, we used the PropGAN architecture to train from a low to a high resolution on the ground truth segmentation maps. During training, we

incrementally added layers to the generator and discriminator to increase the spatial resolution of the generated segmentation maps. Per pixel semantic class labels is the output of the generator. We first created per-pixel likelihood scores of belonging to every semantic label, and then sampled every semantic class per pixel to synthesize segmentation layouts. Then, we used tanh function on the generator's last layer to calculate the per-pixel probability scores, which resulted in probability maps. The synthesized samples fed to the PropGAN discriminator should still have distinct labels, similar to the real samples. As a result, we computed minimax for both forwards and backwards passes, with the goal of achieving practical probability outputs.

C. Generator and Discriminator Architecture

The detailed architectures of the generator and discriminator subnetworks used in our work are shown in Fig. 3. The generator uses the MUNet architecture [40] and it is built from scratch and trained according to our dataset. The upper half corresponds to the contracting encoder arm where resolution decreases and feature depth increases as one proceeds from left to right and the lower half corresponds to the expanding decoder arm where resolution increases and feature depth decreases as one proceeds from right to left. The feature map size for the downscaling and upscaling layers of the generator is listed in Table 1.

TABLE 1
THE DETAILED ARCHITECTURE OF THE GENERATOR SUBNETWORK INCLUDING DOWNSCALING AND UPSCALING PARTS.

Instruction	Layers	Kernel Size	Feature Map Size
Input	Input	-	(Batch size, 512,512,3)
Downscale	Conv2D	4x4	(Batch size, 256,256,32)
	Conv2D		(Batch size, 128,128,64)
	Conv2D		(Batch size, 64,64,128)
	Conv2D		(Batch size, 32,32,256)
Upscale	Deconv2D	4x4	(Batch size, 32,32,256)
	Deconv2D		(Batch size, 64,64,128)
	Deconv2D		(Batch size, 128,128,64)
	Deconv2D		(Batch size, 256,256,32)
Output	Output	-	(Batch size, 512,512,3)

The skip connections characteristic of the U-Net architecture [41] connect corresponding resolution layers between the encoder and decoder arms allowing for the insertion of details in the upsampling for each resolution expansion. Compared to U-Net, the changes in the MUNet architecture include: the introduction of batch normalization, the use of the ReLU activation function in the decoder and Leaky ReLU for the encoder, and elimination of the pooling

layer. Specifically, as shown in Fig. 3, in the contracting arm of the MUNet, we used convolutional layers with a kernel size of 4×4 followed by batch normalization and Leaky ReLU activation function, and in the expanding arm, we used deconvolution layers with a 4x4 stride followed by batch normalization and ReLU activation function. Finally, for mapping every 32-component feature vector to the desired number of classes (road and non-road), we used the final deconvolution layer with the 4x4 stride and a tanh activation function [31] for mapping predicted values to classification probabilities. The ReLU and Leaky ReLU activation functions are, respectively, defined as

$$ReLU(k) = \begin{cases} 0 & \text{if } k \leq 0 \\ k & \text{if } k > 0 \end{cases} \quad (4)$$

$$LReLU(k) = \begin{cases} k & \text{if } k > 0 \\ \alpha k & \text{if } k \leq 0 \end{cases} \quad (5)$$

where α is a small constant between 0.1 and 0.3 [42].

The discriminator architecture used in our work is also shown in Fig. 3. The ground truth data and segmentation results are fed into the discriminative term to find whether the generator output is fake (0) or real (1). The discriminator uses a fully convolutional architecture with 17 layers, with a structure that mimics the encoder arm of the generator comprising of convolutional layers with a kernel size of 4×4 and stride of 2×2 followed by batch normalization and Leaky ReLU activation function. The final layer used a sigmoid function to produce a value between 0 and 1 indicative of the discriminator’s assessment of the probability that the presented road segmentation map corresponds to labeled ground truth [43].

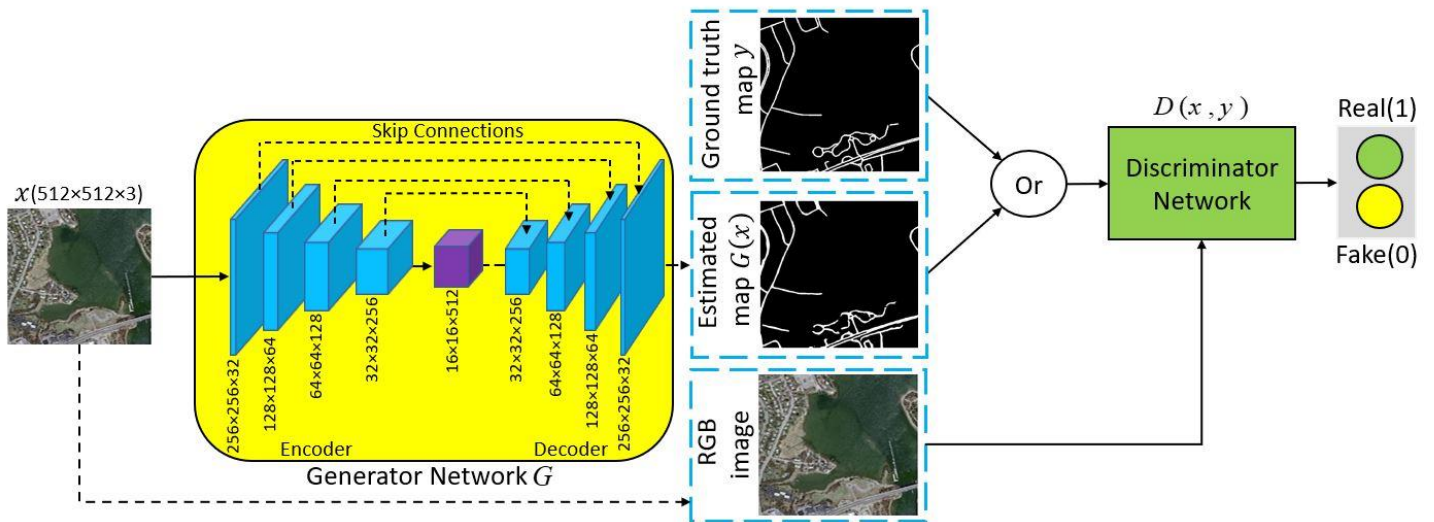


FIGURE 2. GAN training to generate a road segmentation map from an RGB image; the generator network seeks to create a representation that cannot be distinguished from the ground truth image by the discriminator network, which in turn is trained to best distinguish generated samples from real ground truth data.

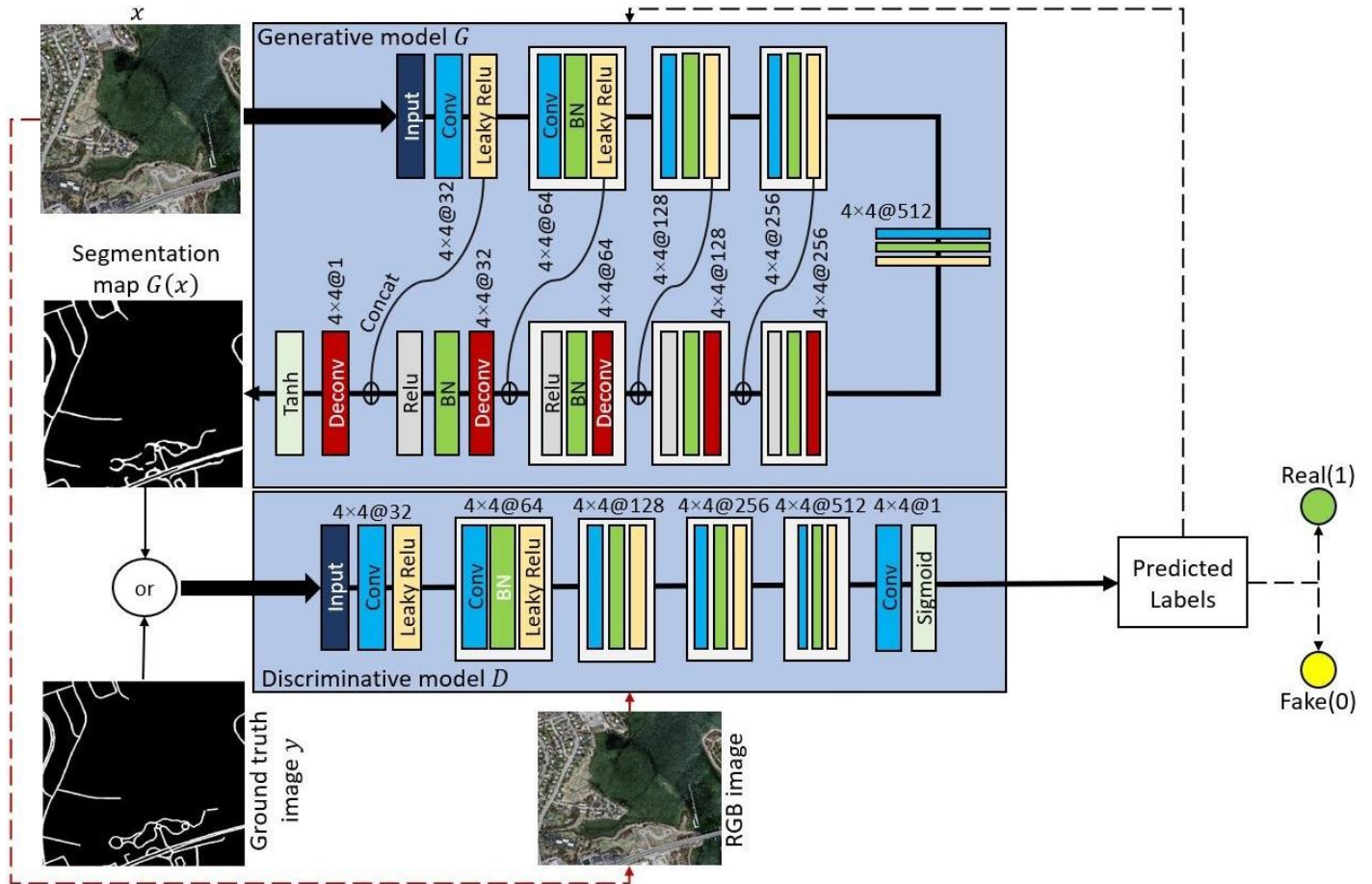


FIGURE 3. Detailed structures of generative and discriminative networks comprising the proposed GAN for road network segmentation.

III. RESULTS

A. Dataset

For our benchmarks, we used the Massachusetts dataset [44], which is the largest existing road dataset. This dataset includes 1,171 aerial images with original spatial dimensions of 1500×1500. For validating the proposed model on the dataset for road extraction, 100 images with complete information and good quality were selected. The original images were divided into eight parts with a size of 512×512 to accommodate computational constraints. Consequently, 761 images were used as the final dataset in the experiments. The dataset was divided into 733 images for training and validation: and 28 images for testing. Data augmentation techniques, such as horizontal flip, vertical flip, zooming, and rotation, were used to increase dataset size for training of the proposed method.

B. Parameters and Implementation

For LLF, the sigma and alpha parameters were set as 0.2 and 0.3, respectively. Training of the GAN network to optimize the loss function was performed using the extensively utilized Adam optimizer [42] with learning rate of 0.001, beta_1 of 0.9 and beta_2 of 0.999. A dropout probability of 0.5 was used during

model training to avoid overfitting. The proposed model was trained with batch size 1 for 100 epochs and the trained model was then applied to the test data to extract roads. The extracted labels were compared against the ground truth labels for evaluating the performance. The whole process of the proposed method for road extraction from remotely sensed imagery was implemented on a GPU Nvidia Quadro P5000 with a computing capacity of 6.1 with 2560 shading units, 160 texture mapping units, and 64 render output units (ROPs), and a memory of 16 GB under the framework of Keras with Tensorflow backend.

C. Performance evaluation metrics

Five metrics were used to evaluate the accuracy assessment of the suggested method applied for road class extraction from high-resolution remote sensing data, namely, F1 score, recall, precision, Matthews correlation coefficient (MCC), and Mean intersection over union (MIOU) factors. These metrics can be calculated from the number of false positive (FP), false negative (FN), true negative (TN), and true positive (TP) pixels as

$$MCC = \frac{TP \cdot TN - FP \cdot FN}{\sqrt{(TP + FP)(TP + FN)(TN + FP)(TN + FN)}}$$

$$Recall = \frac{Tp}{TP + FN}$$

$$Precision = \frac{TP}{TP + FP}$$

$$F1 = \frac{2 \times Precision \times Recall}{Precision + Recall}$$

$$MIOU = \frac{1}{k} \sum_{i=0}^{k-1} \frac{TP_i}{TP_i + FP_i + FN_i}$$

The recall represents the fraction of the labeled road pixels that are correctly classified and precision represents the fraction of the road pixel classifications that are correct [20]. The F1 score [45] combines the precision and recall metrics within a single numeric score that is considered a balanced measure of accuracy when class sizes are different. In addition, the MCC is also a correlation coefficient between predicted and recognized binary classifications, providing a value between -1 and +1 [46]. The proportion of unions and intersections between the set of classified values and the set of ground truth is computed using MIOU. In MIOU, the number of classes k is equal to 2 presenting the road class and background.

D. Experimental results

Figure 4 visually illustrates the results obtained with the proposed MUNet and GAN models for some images with varied characteristics, specifically including non-complex and complex backgrounds, shadows, and occlusions due to trees and buildings. From the results in the figure, one can observe that, while both the proposed approaches can extract and detect roads in the images with good accuracy, the GAN framework offers several advantages over the MUNet approach. The MUNet approach is sensitive to occlusion by trees and to shadows and predicts few FN pixels (depicted in blue box in Fig. 4) but has its accuracy compromised due to a number of FP pixels (depicted in yellow box in Fig. 4). Given that the textural and spectral characteristics of parking lots, shadows, and buildings frequently match those of roads, the proposed MUNet model cannot reliably distinguish roads from these other elements, resulting in incorrect classification for several small patches. Moreover, some of the extracted road parts are not continuous; lack of connectivity is observed between the roads at junction regions where roads connect. For complex images, extracting road parts can be challenging for the proposed MUNet model. The proposed GAN model offers a significant improvement over the MUNet approach and generates more coherent high-resolution road segmentation maps with better preservation of the road borders and mitigation of the effects of occlusions and shadows. Compared to the MUNet approach the GAN approach predicts fewer FP pixels, which is a key contributor to the improved accuracy.

TABLE 2
QUANTITATIVE ACCURACY METRICS FOR THE PROPOSED APPROACHES FOR THE INDIVIDUAL IMAGES IN THE MASSACHUSETTS ROAD DATASET. VALUES ARE REPORTED IN PERCENTAGE, AND THE BEST METRICS ARE INDICATED BY BOLD FONT.

		Prop-MUNet	Prop-GAN
Image 1	Recall	95.80	93.45
	Precision	79.51	86.83
	F1 score	86.90	90.02
	MCC	85.38	88.65
	MIOU	80.02	84.24
Image 2	Recall	94.30	91.25
	Precision	79.66	89.19
	F1 score	86.36	90.21
	MCC	84.29	88.57
	MIOU	79.91	84.91
Image 3	Recall	93.50	91.28
	Precision	84.53	89.70
	F1 score	88.79	90.48
	MCC	86.98	88.91
	MIOU	83.02	85.27
Image 4	Recall	96.88	95.24
	Precision	87.12	92.91
	F1 score	91.74	94.06
	MCC	91.02	93.47
	MIOU	86.24	89.86
Image 5	Recall	94.29	91.86
	Precision	88.99	93.37
	F1 score	91.56	92.61
	MCC	90.38	91.58
	MIOU	86.55	88.04
Image 6	Recall	96.15	93.34
	Precision	89.36	93.63
	F1 score	92.63	93.48
	MCC	91.74	92.66
	MIOU	87.97	89.22
Image 7	Recall	94.15	91.94
	Precision	91.41	95.28
	F1 score	92.76	93.58
	MCC	91.98	92.92
	MIOU	87.87	89.13
Image 8	Recall	95.03	95.02
	Precision	86.83	91.42
	F1 score	90.74	93.19
	MCC	89.60	92.31
	MIOU	88.43	88.82
Average	Recall	95.01	92.92
	Precision	85.92	91.54
	F1 score	90.18	92.20
	MCC	88.92	91.13
	MIOU	85.00	87.43

The accuracy of the proposed MUNet and GAN models was also evaluated numerically in terms of the five metrics defined in Section III B and the results are summarized in Table 2. The numerical results in Table 2 reinforce the findings from the visually presented results in Fig. 4; compared with the MUNet model the GAN model provides significantly higher precision but slightly lower recall, indicating that the MUNet model predicts more false positive and less false negative pixels than the GAN model. For the combined F1 score and MCC accuracy metrics, the GAN model achieves scores of 92.20%, and 91.13%

compared with scores of 90.18%, and 88.92% for the MUNet, respectively. The improvements of 2.02% and 2.21%, respectively, for F1 score and MCC demonstrate the superiority of the proposed GAN approach for road extraction. Although the proposed GAN approach offers state of the art performance, it is also impacted by the complicated backgrounds and occlusions, as well as the challenge of common spatial and spectral characteristics of roads with other regions, such as parking lots, and buildings. We also conducted some experiments to check the effect of different hyper-parameters on the performance of the model for road extraction. We changed the Adam optimizer to Stochastic gradient descent (SGD) with a learning rate of 0.001 and ReLU activation function used in the encoder part of the model to Exponential linear unit (ELU). We then performed the Prop-GAN with these hyper-parameters (Pro-GAN+ELU+SGD) on the dataset. We measured the evaluation metrics for the same test images after adding the SGD and ELU parameters. We achieved an average accuracy of 88.01% for Precision, 92.02% for F1 score, 90.99% for MCC, and 87.25% for MIOU. As it is shown, the Prop-GAN approach with ReLU and Adam parameters (Prop-GAN+ReLU+Adam) obtained better accuracy and improved the results by 3.53%, 0.18%, 0.14%, and 0.18% for Precision, F1 score, MCC, and MIOU, respectively. In contrast, the Prop-GAN+ELU+SGD method obtained 96.43% for Recall compared to the Pro-GAN+ReLU+Adam with 92.92%, which shows that more FPs and fewer FNs were predicted by the method. Furthermore, we depicted some qualitative results of the Prop-GAN+ELU+SGD method in Figure 4 (e). As it can be seen, compared with the same test images in Figure 4 achieved with Prop-GAN+ReLU+Adam, more non-road pixels were predicted by the Prop-GAN+ELU+SGD, which leads to obtaining less accurate qualitative results compared to the Prop-GAN+ReLU+Adam.

IV. COMPARISON AND DISCUSSION

The performance of the proposed MUNet and GAN approaches over the Massachusetts road dataset was also compared against six state-of-the-art prior approaches for road extraction from high

resolution aerial imagery: (1) The SEEDS-MCNN proposed recently by Lv, et al. [47], which uses super-pixels extracted via energy-driven sampling (SEEDS) followed by a CNN classifier, (2) The CNN [18] approach of Zhong, et al. [23](3) The RSRCNN [38] approach of Wei, et al. [48] which uses road structure-refined CNN model that is provided with road geometric information and spatial correlation, (4) The Road-RCF [39] technique proposed by Hong, et al. [49] which uses richer convolutional features (RCFs) for road extraction, (5) the RDRCNN [40] approach proposed by Gao, et al. [50] which uses a novel architecture called the refined deep residual CNN composed of dilated perception and residual connected units, and (6) the RDRCNN+Postprocessing [40] approach of Gao, et al. [50] which performs a post-processing step on the RDRCNN output using mathematical morphology and a tensor-voting method to incorporate split roads. The referenced publications for these prior methods reported precision, recall, and F1 score on the Massachusetts road dataset and those values are compared in Table 3 against the corresponding metrics for the MUNet and GAN approaches proposed in this paper.

TABLE 3
AVERAGE PRECISION, RECALL, AND F1 SCORE METRICS OVER THE MASSACHUSETTS ROAD DATASET FOR THE PROPOSED APPROACH AND ALTERNATIVE TECHNIQUES. FOR EACH METRIC, THE BEST VALUE OBTAINED ACROSS THE DIFFERENT METHODS IS INDICATED BY BOLD FONT.

	Average Percentage		
	Recall	Precision	F1 score
CNN [18]	68.6	43.5	53.2
SEEDS-MCNN [37]	80.4	78.0	79.0
RSRCNN [38]	72.9	60.6	66.2
Road-RCF [39]	98.5	85.8	91.5
RDRCNN [40]	75.33	84.64	79.72
RDRCNN + post-processing [40]	75.75	85.35	80.31
Prop-MUNet	95.01	85.92	90.18
Prop-GAN	92.92	91.54	92.20

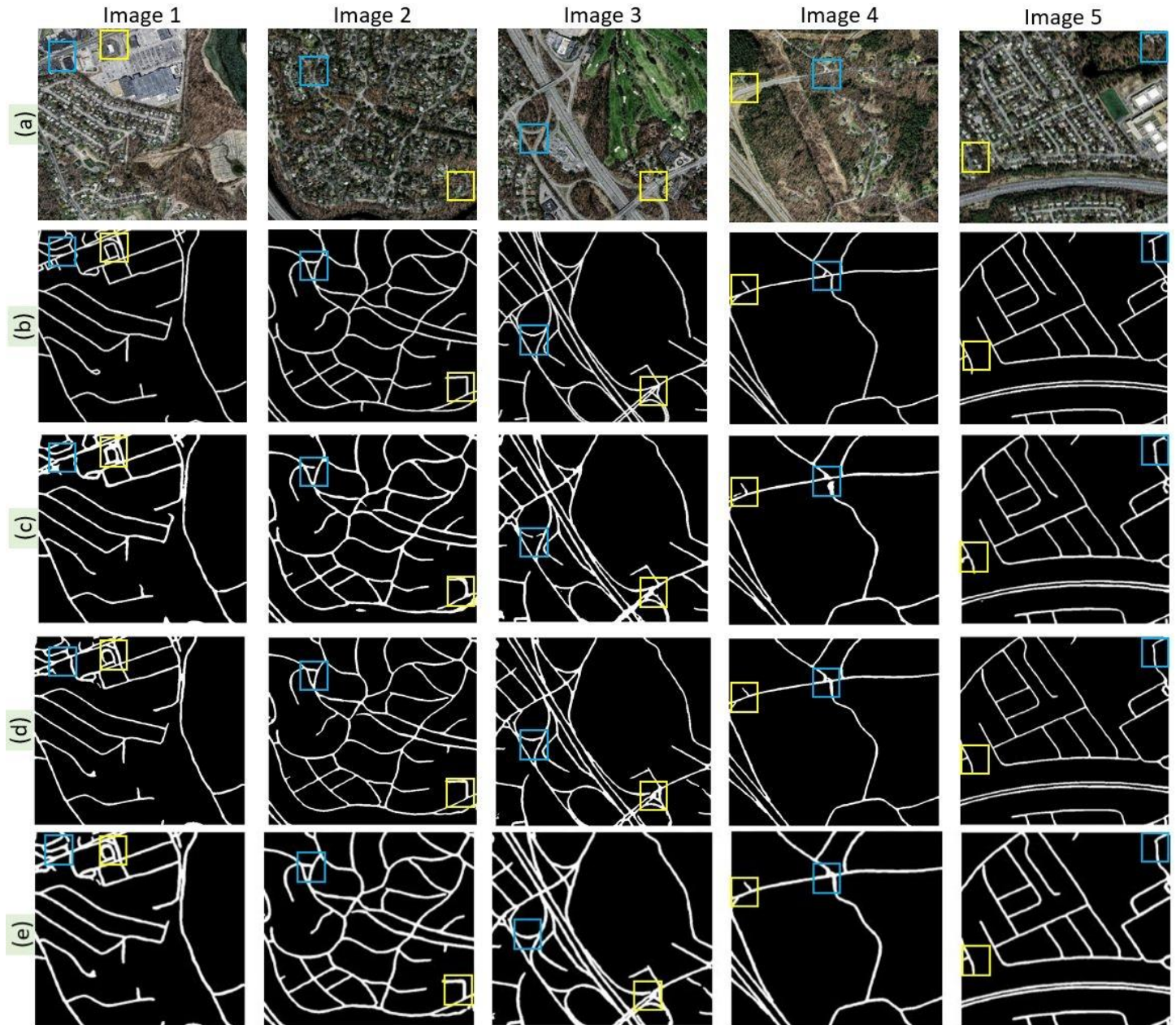


FIGURE 4. Sample image blocks and corresponding extracted road regions using alternative techniques: (a) image block, (b) ground truth road segmentation, (c) road segmentation obtained with the proposed modified U-Net model (Prop-MUNet), (d) road segmentation obtained with the proposed GAN approach (Prop-GAN+ReLU+Adam), and (e) road segmentation obtained with the proposed GAN approach with new parameters (Prop-GAN+ELU+SGD). The blue and yellow boxes present the FNs and FPs, respectively.

The results in Table 3 demonstrate the effectiveness of the proposed GAN approach, which provides the highest F1 score among all the methods compared, which at 92.20% is 0.7% better than the next best performing Road-RCF [39] technique and 2.02% better than the proposed MUNet approach. The proposed GAN approach yields the highest precision metric, which at 91.54% is almost 5.74% better than the next best Road-RCF [39] technique and 5.62% better than the proposed MUNet approach, which has the third best precision value. The proposed GAN

approach also has a high recall metric, which at 92.92% is only superseded by the 98.5% value for the Road-RCF [39] technique but is better than all other prior methods and only slightly worse than the 95.01% value for the proposed MUNet. Among the prior methods, the Road-RCF [39] technique offers performance that is clearly superior to other methods in all three reported metrics. The CNN and RSRCNN achieved the lowest accuracy compared with the other methods and our proposed methods in this paper.

In addition to the numerical results presented in Table 3, we also present a sample set of images and extracted road regions for the images to highlight and compare the performance of the alternative techniques that are depicted in Figure 5. The first and second columns present the test and ground truth images, whereas the third column depict the results achieved by the state-of-the-art SEEDS-MCNN Lv, et al. [47], CNN [18] and RDRCNN [40] methods. The fourth column shows the results

achieved by the state-of-the-art Road-RCF [39], RSRCNN [38] and RDRCNN [40]. Finally, the fifth and sixth columns illustrate the extracted road parts using proposed MUNet and GAN models, respectively. These images further highlight the effectiveness of the proposed GAN approach, which is particularly effective in preserving the edges of the roads while maintaining high fidelity with the ground truth labels.

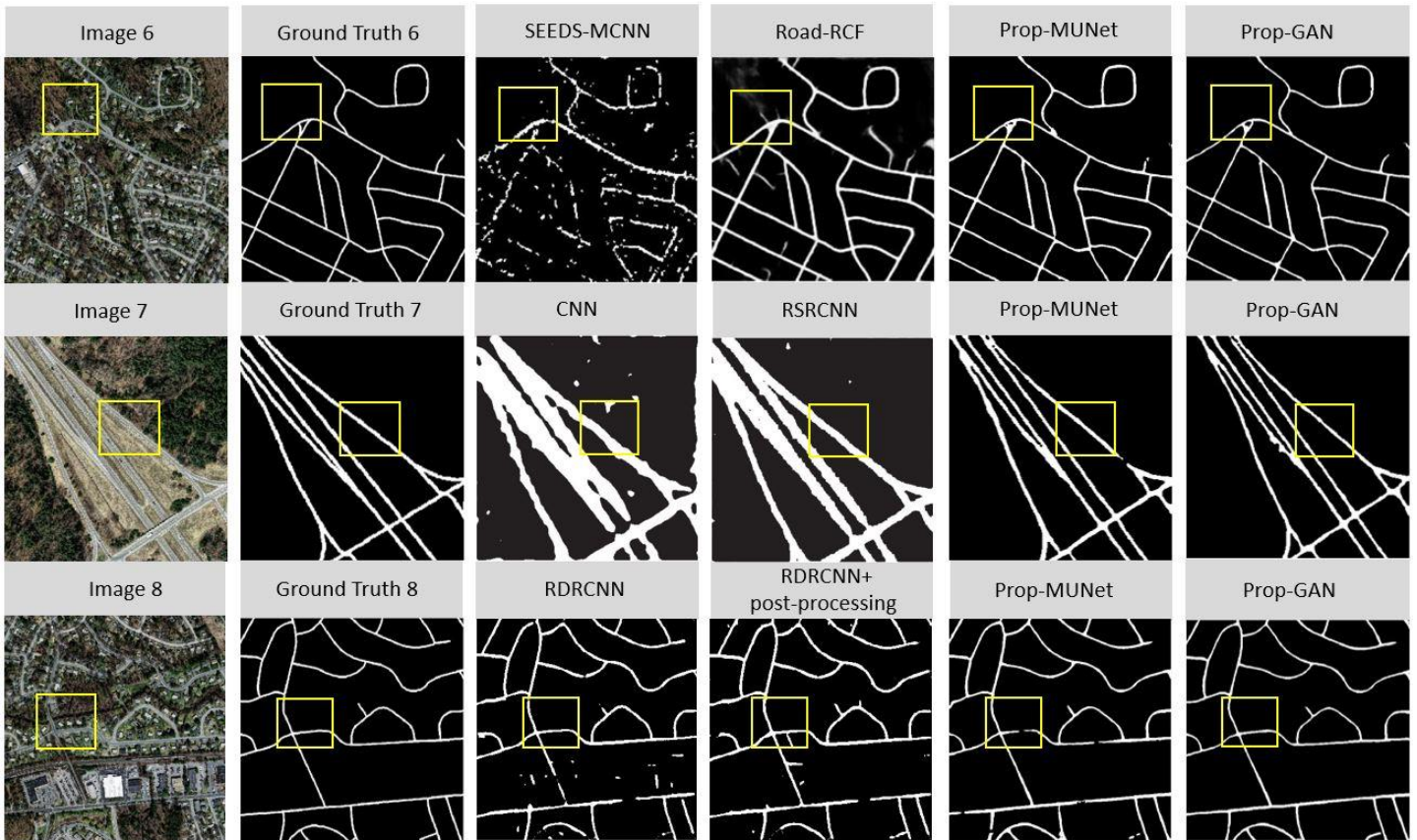


FIGURE 5. Comparison of road segmentation obtained with the proposed method (GAN) against other techniques illustrated on the three images from the Massachusetts road dataset. The yellow boxes highlight regions with the FP and FN pixel predictions by the models.

Also, we compared the performance of the proposed GAN+MUNet approach with other GAN-based road extraction approaches reported in the literature such as GAN+FCN [32], GAN+SegNet [21], E-WGAN [33], MsGAN [34], and McGAN [35] to test the efficacy of the presented model in road extraction. For comparison purpose, that the statistical measure such as the accuracy, recall, and F1 scores reported in the referenced papers vs. our proposed Prop-GAN approach are shown in Table 4. The quantitative results indicate that the presented GAN+MUNet model attained the highest F1 score value with 92.20%, which could improve the earlier methods by 2.57% compared to the second highest approach called GAN+SegNet. Also, the model could improve the F1 score value compared to the other GAN-based road extraction methods such as GAN+FCN, E-WGAN, MsGAN, and

McGAN to 5.2%, 7.2%, 6%, and 7.3%, respectively, assert the GAN+MUNet model's ability to extract roads from aerial imagery. Also, we estimated the runtime of the suggested approach applied on the dataset, which took 78.6s per epoch and 71ms per step for training and testing process, respectively. The model was trained for 100 epochs and tested on 28 images; thus, it took 131 minutes for training and 2s for testing. Overall, the proposed model does not require high computational time and a large training dataset and still achieved the best performance among other comparative models in term of both quantitative and qualitative results.

TABLE 4
AVERAGE PRECISION, RECALL, AND F1 SCORE METRICS FOR THE PROPOSED GAN+MUNET AND ALTERNATIVE GAN-BASED ROAD DETECTION APPROACHES. BOLD FONT INDICATES THE BEST VALUE.

	Average Percentage		
	Recall	Precision	F1 score
GAN+FCN	82	93	87
GAN+SegNet	91.01	88.31	89.63
E-WGAN	85	86	85
MsGAN	87.1	85.3	86.2
McGAN	85.8	84.1	84.9
Prop-GAN	92.92	91.54	92.20

IV. CONCLUSION

We proposed a deep learning approach for segmenting road regions from high-resolution images that incorporates two new innovations: a modified U-Net (MUNet) architecture for the extraction of road regions and a generative adversarial neural network (GAN) framework for optimizing learning and improving the accuracy of the segmentation map. Experimental results validated the efficacy of the proposed approach. Compared with prior state-of-the-art approaches and GAN-based road detection methods, the proposed GAN framework offers significant improvements in precision and in the F1 score metrics. Visual comparison indicates that the proposed GAN approach yields high-quality segmentation maps where, compared with prior approaches, the edges are particularly well preserved and in agreement with ground truth labels. However, the accuracy of the proposed deep learning model is slightly lower, and the method could neither identify roads from complex areas nor extract continuous road parts from these images. These factors are the main limitations of the proposed GAN method. Future research can address these limitations and use some topological characteristics like connectivity or curvature and slope to improve the accuracy of our proposed approach for road extraction.

AUTHOR CONTRIBUTIONS

Conceptualization, A.A. and B.P.; methodology and formal analysis, A.A.; data curation, A.A.; writing—original draft preparation, A.A.; writing—review and editing, B.P., G.S.; supervision, B.P., G.S.; funding – B.P., K.N.A.M, and A.A.A., All authors have read and agreed to the published version of the manuscript.

CONFLICT OF INTEREST

The authors declare no conflict of interest.

REFERENCE

- [1] Z. Miao, B. Wang, W. Shi, and H. Zhang, "A semi-automatic method for road centerline extraction from VHR images," *IEEE Geoscience and Remote Sensing Letters*, vol. 11, no. 11, pp. 1856-1860, 2014.
- [2] W. Wang, N. Yang, Y. Zhang, F. Wang, T. Cao, and P. Eklund, "A review of road extraction from remote sensing images," *Journal of Traffic Transportation Engineering*, vol. 3, no. 3, pp. 271-282, 2016.
- [3] N. A. Nasir, K. N. Maulud, and N. I. Yusoff, "Geospatial analysis of road distresses and the relationship with the slope factor," *Journal of Engineering Science Technology*, vol. 11, no. 5, pp. 655-665, 2016.
- [4] M. A. S. Bahri, K. N. A. Maulud, M. A. Rahman, A. O. R. Oon, and C. H. C. Hashim, "Integrated facility and assets management using gis-web application," in *IOP Conference Series: Earth and Environmental Science*, vol. 540, no. 1, pp. 012068, 2020.
- [5] A. Abdollahi and B. Pradhan, "Integrated technique of segmentation and classification methods with connected components analysis for road extraction from orthophoto images," *Expert Systems with Applications*, pp. 114908, 2021.
- [6] A. Katartzis and H. Sahli, "A stochastic framework for the identification of building rooftops using a single remote sensing image," *IEEE Transactions on Geoscience Remote Sensing*, vol. 46, no. 1, pp. 259-271, 2007.
- [7] J. Zhang, L. Chen, L. Zhuo, W. Geng, and C. Wang, "Multiple saliency features based automatic road extraction from high-resolution multispectral satellite images," *Chinese Journal of Electronics*, vol. 27, no. 1, pp. 133-139, 2018.
- [8] A. Buslaev, S. Seferbekov, V. Iglovikov, and A. Shvets, "Fully convolutional network for automatic road extraction from satellite imagery, IEEE/CVF Conference on Computer Vision and Pattern Recognition Workshops (CVPRW), pp. 207-210, 2018. <https://doi.org/10.1109/CVPRW.2018.00035>.
- [9] T. Su, T. Liu, S. Zhang, Z. Qu, and R. Li, "Machine learning-assisted region merging for remote sensing image segmentation," *ISPRS Journal of Photogrammetry Remote Sensing*, vol. 168, pp. 89-123, 2020.
- [10] Y. Zhang, Z. Lu, D. Ma, J.-H. Xue, and Q. Liao, "Ripple-GAN: Lane line detection with ripple lane line detection network and Wasserstein GAN," *IEEE Transactions on Intelligent Transportation Systems*, 2020. <https://doi.org/10.1109/TITS.2020.2971728>.
- [11] G. Cheng and J. Han, "A survey on object detection in optical remote sensing images," *ISPRS Journal of Photogrammetry Remote Sensing*, vol. 117, pp. 11-28, 2016.
- [12] W. H. M. Wan Mohtar, A. M. Muad, M. Porhemmat, H. Ab. Hamid, and S. S. Whayab, "Measuring scour level based on spatial and temporal image analyses," *Structural Control Health Monitoring*, vol. 28, no. 1, pp. e2645, 2021.
- [13] J. Long, E. Shelhamer, and T. Darrell, "Fully convolutional networks for semantic segmentation," in *Proceedings of the IEEE Conference on Computer Vision and Pattern Recognition*, vol. 39, no. 4, pp. 3431-3440, 2015.
- [14] S. Zhang, Q. Yuan, J. Li, J. Sun, and X. Zhang, "Scene-adaptive remote sensing image super-resolution using a multiscale attention network,"

- IEEE Transactions on Geoscience Remote Sensing*, vol. 58, no. 7, pp. 4764-4779, 2020.
- [15] H. Kamangir, M. Momeni, and M. Satari, "Automatic centerline extraction of covered roads by surrounding objects from high resolution satellite images," *ISPRS-International Archives of the Photogrammetry, Remote Sensing Spatial Information Sciences*, pp. 111-116, 2017.
- [16] A. Abdollahi, B. Pradhan, and N. Shukla, "Extraction of road features from UAV images using a novel level set segmentation approach," *International Journal of Urban Sciences*, pp. 1-15, 2019.
- [17] R. Alshehhi and P. R. Marpu, "Hierarchical graph-based segmentation for extracting road networks from high-resolution satellite images," *ISPRS Journal of Photogrammetry and Remote Sensing*, vol. 126, pp. 245-260, 2017.
- [18] Z. Da-Ming, W. Xiang, and L. Chun-Li, "Road extraction based on the algorithms of MRF and hybrid model of SVM and FCM," in *Image and Data Fusion (ISIDF), International Symposium on Image and Data Fusion*, Tengchong, Yunnan, China, pp. 1-4, 2011.
- [19] C. Unsalan and B. Sirmacek, "Road network detection using probabilistic and graph theoretical methods," *IEEE Transactions on Geoscience and Remote Sensing*, vol. 50, no. 11, pp. 4441-4453, 2012.
- [20] H. R. R. Bakhtiari, A. Abdollahi, and H. Rezaeian, "Semi automatic road extraction from digital images," *The Egyptian Journal of Remote Sensing and Space Science*, vol. 20, no. 1, pp. 117-123, 2017.
- [21] Q. Shi, X. Liu, and X. Li, "Road detection from remote sensing images by generative adversarial networks," *IEEE Access*, vol. 6, pp. 25486-25494, 2018.
- [22] A. Abdollahi, B. Pradhan, N. Shukla, S. Chakraborty, and A. Alamri, "Deep learning approaches applied to remote sensing datasets for road extraction: A state-of-the-art review," *Remote Sensing*, no. 12, pp. 1444, 2020.
- [23] Z. Zhong, J. Li, W. Cui, and H. Jiang, "Fully convolutional networks for building and road extraction: Preliminary results," in *2016 IEEE International Geoscience and Remote Sensing Symposium (IGARSS)*, Beijing, China, pp. 1591-1594, 2016.
- [24] W. S. Wan Mohd Jaafar *et al.*, "Improving individual tree crown delineation and attributes estimation of tropical forests using airborne LiDAR data," *Forests*, vol. 9, no. 12, pp. 759, 2018.
- [25] J. Wang, J. Song, M. Chen, and Z. Yang, "Road network extraction: A neural-dynamic framework based on deep learning and a finite state machine," *International Journal of Remote Sensing*, vol. 36, no. 12, pp. 3144-3169, 2015.
- [26] P. Li *et al.*, "Road network extraction via deep learning and line integral convolution," in *IEEE International Geoscience and Remote Sensing Symposium (IGARSS), Beijing, China, pp. 1599-1602, 2016. <https://doi.org/10.1109/IGARSS.2016.7729408>*.
- [27] T. Panboonyuen, P. Vateekul, K. Jitkajornwanich, and S. Lawawirojwong, "An enhanced deep convolutional encoder-decoder network for road segmentation on aerial imagery," in *International Conference on Computing and Information Technology*, Springer, pp. 191-201, 2017. https://doi.org/10.1007/978-3-319-60663-7_18.
- [28] Y. Wang, J. Seo, and T. Jeon, "NL-LinkNet: Toward lighter but more accurate road extraction with nonlocal operations," *IEEE Geoscience Remote Sensing Letters*, 2021. <https://doi.org/10.1109/LGRS.2021.3050477>.
- [29] G. Cheng, Y. Wang, S. Xu, H. Wang, S. Xiang, and C. Pan, "Automatic road detection and centerline extraction via cascaded end-to-end convolutional neural network," *IEEE Transactions on Geoscience Remote Sensing*, vol. 55, no. 6, pp. 3322-3337, 2017.
- [30] Y. Xu, Z. Xie, Y. Feng, and Z. Chen, "Road extraction from high-resolution remote sensing imagery using deep learning," *Remote Sensing*, vol. 10, no. 9, pp. 1461, 2018.
- [31] P. Luc, C. Couprie, S. Chintala, and J. Verbeek, "Semantic segmentation using adversarial networks," 2016. Available from: <https://arxiv.org/abs/1611.08408>.
- [32] X. Zhang, X. Han, C. Li, X. Tang, H. Zhou, and L. Jiao, "Aerial image road extraction based on an improved generative adversarial network," *Remote Sensing*, vol. 11, no. 8, pp. 930, 2019.
- [33] C. Yang and Z. Wang, "An ensemble wasserstein generative adversarial network method for road extraction from high resolution remote sensing images in rural areas," *IEEE Access*, vol. 8, pp. 174317-174324, 2020.
- [34] Y. Zhang, Z. Xiong, Y. Zang, C. Wang, J. Li, and X. Li, "Topology-aware road network extraction via multi-supervised generative adversarial networks," *Remote Sensing*, vol. 11, no. 9, pp. 1017, 2019.
- [35] Y. Zhang, X. Li, and Q. Zhang, "Road topology refinement via a multi-conditional generative adversarial network," *Sensors*, vol. 19, no. 5, pp. 1162, 2019.
- [36] M. Aubry, S. Paris, S. W. Hasinoff, J. Kautz, and F. Durand, "Fast local laplacian filters: Theory and applications," *ACM Transactions on Graphics*, vol. 33, no. 5, pp. 167, 2014.
- [37] S. Paris, S. W. Hasinoff, and J. Kautz, "Local laplacian filters: Edge-aware image processing with a laplacian pyramid," *ACM Trans. Graph.*, vol. 30, no. 4, pp. 68, 2011.
- [38] I. Goodfellow *et al.*, "Generative adversarial nets," in *Advances in Neural Information Processing Systems*, pp. 2672-2680, 2014.
- [39] L. Ding, M. H. Bawany, A. E. Kuriyan, R. S. Ramchandran, C. C. Wykoff, and G. Sharma, "A novel deep learning pipeline for retinal vessel detection in fluorescein angiography," *IEEE Transactions on Image Processing*, 2020. <https://doi.org/10.1109/TIP.2020.2991530>.
- [40] Y. Enokiya, Y. Iwamoto, Y.-W. Chen, and X.-H. Han, "Automatic liver segmentation using u-net with wasserstein GANs," *Journal of Image Graphics*, vol. 6, no. 2, pp. 152-159, 2018.
- [41] O. Ronneberger, P. Fischer, and T. Brox, "U-net: Convolutional networks for biomedical image segmentation," in *International Conference on Medical Image Computing and Computer-Assisted Intervention*, pp. 234-241, 2015.
- [42] Q. Zhang, Z. Cui, X. Niu, S. Geng, and Y. Qiao, "Image segmentation with pyramid dilated convolution based on ResNet and U-Net," in *International Conference on Neural Information Processing*, pp. 364-372, 2017. https://doi.org/10.1007/978-3-319-70096-0_38.

- [43] A. Abdollahi, B. Pradhan, and N. Shukla, "Road extraction from high-resolution orthophoto images using convolutional neural network," *Journal of the Indian Society of Remote Sensing*, pp. 1-15, 2020.
- [44] V. Mnih, Machine learning for aerial image labeling, *Ph.D. dissertation, Dept. Comput. Sci., Univ. Toronto, Toronto, ON, Canada*. Citeseer, 2013.
- [45] C. Henry, S. M. Azimi, and N. Merkle, "Road segmentation in sar satellite images with deep fully convolutional neural networks," *IEEE Geoscience Remote Sensing Letters*, no. 99, pp. 1-5, 2018.
- [46] A. Abdollahi, B. Pradhan, and A. Alamri, "VNet: An end-to-end fully convolutional neural network for road extraction from high-resolution remote sensing data," *IEEE Access*, vol. 8, pp. 179424 - 179436, 2020.
- [47] X. Lv, D. Ming, Y. Chen, and M. Wang, "Very high resolution remote sensing image classification with SEEDS-CNN and scale effect analysis for superpixel CNN classification," *International Journal of Remote Sensing*, vol. 40, no. 2, pp. 506-531, 2019.
- [48] Y. Wei, Z. Wang, and M. Xu, "Road structure refined cnn for road extraction in aerial image," *IEEE Geosci. Remote Sensing Lett.*, vol. 14, no. 5, pp. 709-713, 2017.
- [49] Z. Hong, D. Ming, K. Zhou, Y. Guo, and T. Lu, "Road extraction from a high spatial resolution remote sensing image based on richer convolutional features," *IEEE Access*, vol. 6, pp. 46988-47000, 2018. <https://doi.org/10.1109/ACCESS.2018.2867210>.
- [50] L. Gao, W. Song, J. Dai, and Y. Chen, "Road extraction from high-resolution remote sensing imagery using refined deep residual convolutional neural network," *Remote Sensing*, vol. 11, no. 5, pp. 552, 2019.



ABOLFAZL ABDOLLAHI received a B.Sc degree from Ferdowsi University of Mashhad, Iran and an M.Sc degree in GIS and Remote Sensing from Kharazmi University of Tehran, Iran. He is currently a PhD student with the Centre for Advanced Modelling and Geospatial Information Systems (CAMGIS), University of Technology Sydney (UTS). His research interests contain the application of advance machine

learning approaches and deep learning-based networks for remote sensing image classification, image segmentation, feature extraction, and GIS maps database updating. He was rewarded the International Research Scholarship and UTS Presidents' Scholarship for the current course in 2018. He has published numerous peer-reviewed papers on the application of machine learning approaches.



BISWAJEET PRADHAN (M'12, SM'16) received the Habilitation degree in remote sensing from the Dresden University of Technology, Germany, in 2011. He is currently the Director of the Centre for Advanced Modelling and Geospatial Information Systems (CAMGIS), Faculty of Engineering and IT. He is also the Distinguished Professor with the University of Technology Sydney. He is also an

internationally established Scientist in the fields of geospatial information systems (GIS), remote sensing and image processing, complex modeling/geo-computing, machine learning and soft-computing applications, natural hazards, and environmental modeling. Since 2015, he has been serving as the Ambassador Scientist for the Alexander Humboldt Foundation, Germany. Out of his more than 650 articles, more than 500 have been published in science citation index (SCI/SCIE) technical journals. He has authored eight books and 13 book chapters. He was a recipient of the Alexander von Humboldt Fellowship from Germany. He received 55 awards in recognition of his

excellence in teaching, service, and research, since 2006. He was also a recipient of the Alexander von Humboldt Research Fellowship from Germany. From 2016 to 2020, he was listed as the World's Most Highly Cited Researcher by Clarivate Analytics Report as one of the world's most influential mind. In 2018-2020, he was awarded as the World Class Professor by the Ministry of Research, Technology and Higher Education, Indonesia. He is also an Associate Editor and an Editorial Member of more than eight ISI journals. He has widely travelled abroad, visiting more than 52 countries to present his research findings.



GAURAV SHARMA, Gaurav Sharma is with the University of Rochester, where he is a Professor in the Department of Electrical and Computer Engineering, Department of Computer Science, and Department of Biostatistics and Computational Biology. He is also a Distinguished Researcher in Center of Excellence in Data Science (CoE) at the Goergen Institute for Data Science. From 2008-2010, he served as the Director for the Center for Emerging and Innovative Sciences (CEIS), a New York state supported center for

promoting joint university-industry research and technology development, which is housed at the University of Rochester. From 1996 through 2003, he was with Xerox Research and Technology in Webster, NY first as a member of research and technology staff and then as a Principal Scientist and Project Leader. He received the Ph.D. in Electrical and Computer Engineering from North Carolina State University, Raleigh, NC, and master's degrees in Applied Mathematics from NCSU and in Electrical Communication Engineering from the Indian Institute of Science, Bangalore, India. He received his Bachelor of Engineering degree in Electronics and Communication Engineering from Indian Institute of Technology, Roorkee (formerly, Univ. of Roorkee). Dr. Sharma is a fellow of the IEEE, and a fellow of the Society for Imaging Science and Technology (IS&T). Dr. Sharma is a 2020-21 Distinguished Lecturer of the IEEE Signal Processing Society and a SPIE Visiting Lecturer. Dr. Sharma is the Editor-in-Chief for the IEEE Transactions on Image Processing.



ABULLAH ALAMRI, M.S.; is a professor of earthquake seismology, Director of Seismic Studies Center at King Saud University (KSU). He is the President of the Saudi Society of Geosciences and editor-in-chief of the Arabian Journal of Geosciences (AJGS). He holds a B.S. in geology (1981) from King Saud University, M.Sc. (1985) in applied geophysics from University of South Florida, Tampa and Ph.D (1990) in earthquake seismology from University of Minnesota, USA. He is a member of Seismological

Soc. of America, American Geophysical Union, European Ass. for Environmental & Eng. Geophysics, Earthquakes Mitigation in the Eastern Mediterranean Region, National Comm. for Assessment & Mitigation of Earthquake Hazards in Saudi Arabia, Mitigation of Natural Hazards Com at Civil Defense. His research interests are in the area of crustal structures and seismic micro zoning of the Arabian Peninsula. His recent projects also involve applications of EM and MT in deep groundwater exploration of Empty Quarter and geothermal prospecting of volcanic Harrats in the Arabian shield. He has published more than 150 research papers, achieved more than 45 research projects as well as authored several books and technical reports. He is a principal and Co-investigator in several national and international projects (KSU, KACST, NPST, IRIS, CTBTO, US Air force, NSF, UCSF, LLNL, OSU, PSU and Max Planck). He has also chaired and co-chaired several SSG, GSF, RELEMR workshops and forums in the Middle East. He obtained several worldwide prizes and awards for his scientific excellence and innovation.



Sr. Dr. Khairul Nizam Abdul Maulud is an Assoc. Prof. at the Faculty of Engineering & Built Environment, Universiti Kebangsaan Malaysia. He also appointed as a Head of Earth Observation Centre, Institute of Climate Change, Universiti Kebangsaan Malaysia. He joins the Universiti Kebangsaan

Malaysia since 2001 after completing his B.Sc of Geoinformatics from the University of Technology, Malaysia. He received his M.Sc in Geoinformatics from the University of Technology, Malaysia and PhD in Civil & Structural from Universiti Kebangsaan Malaysia. Currently, he has published more than 86 journal papers, 28 books and chapters in book and 78 proceedings in national and international proceedings. He has involved as a principal researcher and consultant works more than 50 research grants, 33 consultant works in Malaysia. To date, he has supervised 13 PhD students, 6 Master Students and

19 bachelor degrees. His expertise is a Geographical Information System and Geomatic and has almost 20 years' experience in research and consultancy. He has successfully completed almost 17 water-related projects including sea-level rise, geospatial analysis, land-use changes, water quality, shoreline erosion, water management using GIS and Coastal Vulnerability Index. He now led high impact research on climate change, especially on the physical and economic impacts.